ADVANCED ENERGY MATERIALS
www.advenergymat.de

A Piezo-Tribovoltaic Nanogenerator with Ultrahigh Output Power Density and Dynamic Sensory Functions

Siyao Qin, Jiaqi Chen, Peng Yang, Zhaoqi Liu, Xinglin Tao, Xuanyi Dong, Jun Hu, Xiangcheng Chu, Zhong Lin Wang,* and Xiangyu Chen**

Tribovoltaic nanogenerator (TVNG) mainly collects energy from sliding motions of two semiconducting materials, but it cannot effectively react to the pressure change in the vertical direction. Here, a piezo-tribovoltaic nanogenerator (P-TVNG) is proposed by integrating piezoelectric and tribovoltaic effects to collect energy from both the sliding motion and the variation of applied pressure. Hence, this P-TVNG can gain extra performance improvement on the top of the original output limit of TVNG. The maximum output power density of P-TVNG is up to 3.61 W m^{-2}, which is 28.9 % higher than the highest record of the TVNG using similar materials. Additionally, the piezo-module can work as a separated sensory component by switching the circuit, which can monitor and analyze various working parameters of TVNG. A series of dynamic characteristics of TVNG during its operation have been identified, including the hysteresis between output current and applied pressure, the influence and incompatibility of interface stress to output performance, and so on. As a multifunction of devices, this P-TVNG system is possible to be applied in semiconductor industry, smart manufacturing, and many other fields. This work improves the performance of the TVNGs while extending its functionality, which broadens the application field of TVNG devices.

1. Introduction

Entering the era of the Internet of Things (IoT) and Big Data, the large number of miniaturized electronic devices puts forward higher requirements for energy miniaturization, energy saving and environmental protection. Aiming at this urgent challenge, the triboelectric nanogenerator (TENG) was proposed in 2012,[1] which utilizes the triboelectric effect to collect mechanical energy from all kinds of frictional motion on diversified interfaces.[2–6] In recent years, the study of triboelectric materials has also intersected with the field of semiconductors, where the direct-current (DC) output can be generated by using the Schottky contact on the surface of the semiconductor,[7–33] namely the tribovoltaic effect.[18,22] Compared with the traditional TENGs, the tribovoltaic nanogenerators (TVNGs) feature low impedance and high current density, and does not require additional rectifier circuit. A series of progress has been made to continuously improve the output performance of TVNGs. For example, it is reported for the first time that the sliding of a metal needle tip on the two-dimensional semiconductor MoS_2 can generate a short-circuit current (I_{sc}) of tens of nA[7] and this current record has been updated to 340 μA based on the heterojunction of Bi_2Te_3 and GaN.[34] However, TVNGs require closed contact between the triboelectric layers and they cannot effectively collect the energy from longitudinal vibration and separation motions, which is different from TENG devices. This strong dependence on a single motion mode (sliding motion) not only limits its adaptability in the actual working scenario, but also hinders the continued improvement of output power.

At the same time, hybrid energy harvesters based on the tribovoltaic effect in combination with other energy conversion effects are also a potential solution to increase the efficiency of TVNG energy harvesting as well as to improve its adaptability. Previously, the photovoltaic effect is the first choice to couple with the tribovoltaic effect, leading to a significant improvement in the output performance of the devices.[35–40] On the other hand, the piezoelectric effect is capable of generating an electrical signal in response to applied stress, while the related

S. Qin, P. Yang, Z. Liu, X. Tao, X. Dong, J. Hu, Z. L. Wang, X. Chen
CAS Center for Excellence in Nanoscience
Beijing Institute of Nanoenergy and Nanosystems
Chinese Academy of Sciences
Beijing 100083, China
E-mail: zhong.wang@mse.gatech.edu; chenxiangyu@binn.cas.cn

S. Qin, P. Yang, Z. Liu, X. Tao, X. Dong, J. Hu, X. Chen
School of Nanoscience and Engineering
University of Chinese Academy of Sciences
Beijing 100049, China

J. Chen, X. Chu
State Key Laboratory of New Ceramics and Fine Processing
School of Material Science and Engineering
Tsinghua University
Beijing 100084, China
E-mail: chuxiangcheng@mail.tsinghua.edu.cn

Z. L. Wang
School of Materials Science and Engineering
Georgia Institute of Technology
Atlanta, GA 30332-0245, USA

The ORCID identification number(s) for the author(s) of this article can be found under https://doi.org/10.1002/aenm.202303080

DOI: 10.1002/aenm.202303080

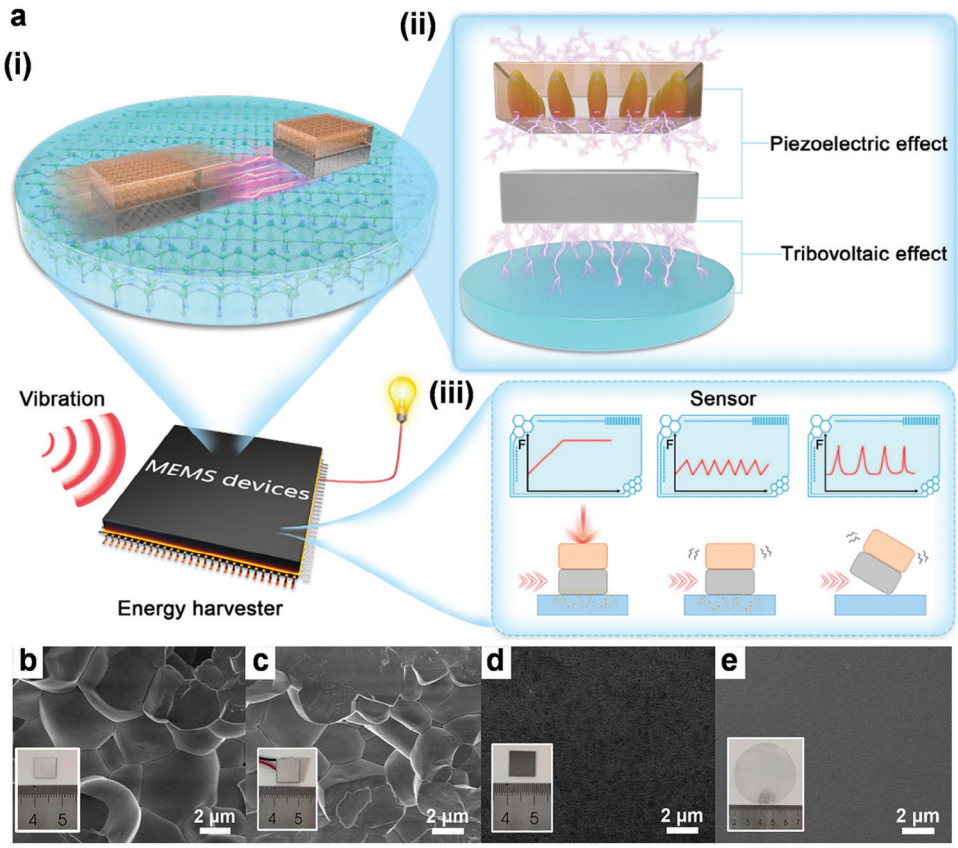

Figure 1. The overall design and materials of the P-TVNG system. a) The structure and energy harvesting function (i), principles (ii) and sensory function (iii) of P-TVNG. b–e) The SEM images and photographs of PZT ceramics (d_{15}, b, and d_{33}, c), Si d), and GaN e).

piezoelectric devices have been intensively applied in the field of energy generation[41–45] and pressure/vibration sensing.[46–49] In this case, the combination of piezoelectric and tribovoltaic effects is capable of responding to diversified friction/vibration motions. However, to our best knowledge, the hybrid energy devices combining the piezoelectric effect with the tribovoltaic effect have not yet been reported. Piezoelectric devices respond primarily to the increase and release of stress while tribovoltaic devices respond primarily to the displacement in the horizontal direction, suggesting that the appropriate system design is the key point to balance the two effects.

Herein, for the first time, we propose a piezo-tribovoltaic generator (P-TVNG), which can achieve extra performance improvement on the top of the original output limit of TVNGs. For P-TVNG, floating-zone silicon (fz-Si, resistivity>1000 Ω m) and ultralow-doped gallium nitride (GaN, doping concentrations $\approx 10^{13}$ cm^{-3}) are the triboelectric materials, while the commercial $Pb(Zr,Ti)O_3$ (PZT) ceramic is the piezoelectric element. The hybrid electrical signal is modulated by a switchable management circuit connecting with the piezoelectric module (piezo-module) and tribovoltaic module (tribo-module). Two kinds of working modes are proposed to solve the compatibility problem of the tribovoltaic and piezoelectric effects, which allow the piezoelectric effect to provide additional energy generation without interfering with the original working performance of the TVNG. In this case, the piezo-module can help to improve the output performance of all kinds of tribovoltaic devices. Moreover, the piezo-module serves the dual function of energy harvesting and motion sensing in this composite system. By switching the management circuits, the piezo-voltage can be used as a sensing signal to characterize the motion state of the tribovoltaic device as well as the stability of the system, which can help to optimize the energy conversion efficiency of the TVNG. This study promotes the application of the TVNG in the semiconductor industry, while the piezo-tribovoltaic coupling effect also brings new applications in the field of electromechanical engineering, smart manufacturing, and so on.

2. Result and discussion

To efficiently collect the mechanical energy from intricate vibrations and motions, the tribovoltaic effect and the piezoelectric effect are integrated into a P-TVNG system, as shown in **Figure 1a**. The system contains a piezo-module and a tribo-module, both capable of generating energy in response to different mechanical motions. Furthermore, the use of semiconductors and piezoelectric ceramics facilitates device miniaturization and enables integration into Micro-electro Mechanical Systems (MEMS) devices, as illustrated in Figure 1a(i). The system incorporates a tightly bonded interface and a movable interface to activate two effects, as demonstrated in Figure 1a(ii). The interface between the piezo-module and a triboelectric semiconductor is closely bonded, ensuring efficient transfer of pressure change and inducing the

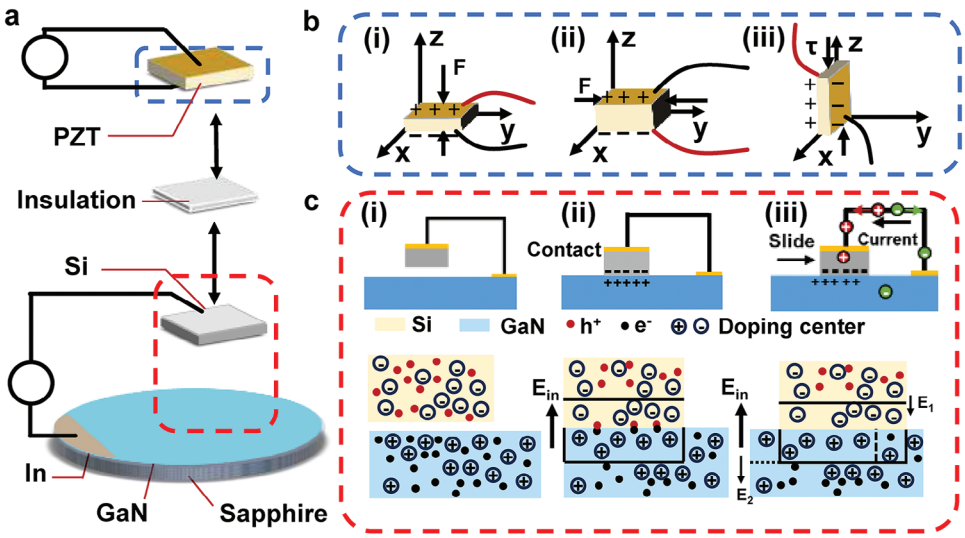

Figure 2. The working mechanism of the P-TVNG system. a) The structure diagram of the P-TVNG. b) Direction of mechanical loading and bound charges generation of the PZT ceramic. c) Distribution of charged particles and electric fields in the prosses of separation (i), contacting (ii) and sliding (iii) of the tribovoltaic materials.

piezoelectric effect. On the other hand, the movable interface allows the tribovoltaic effect to generate electric energy from the sliding motion of the triboelectric semiconductors. In addition, Figure 1a(iii) elucidates the sensory function of the P-TVNG system, wherein the operational state of the device can be monitored by analyzing different signal waveforms under various vibration conditions. The SEM images and detailed photographs of samples are shown in Figure 1b–e. Both d_{15}-PZT and d_{33}-PZT ceramics exhibit large grain sizes and minimal grain boundaries, resulting in less hindrance to domain rotation during polarization and consequently, a larger remanent polarization. In the remanent polarization state, the lattice can respond more rapidly and generate a greater amount of charge under external forces, thereby exhibiting large d_{15} and d_{33} coefficients.[50] The detailed structure of the GaN thin film and PZT ceramic are depicted in Figure S1 (Supporting Information) and the atomic force microscope (AFM) topographic images of GaN and fz-Si are shown in Figures S2 and S3 (Supporting Information).

The working mechanism of the P-TVNG system is shown in **Figure 2a**, where the individual functions and contributions of the piezo-module and tribo-module are explained. The piezo-module consists of a PZT ceramic with silver electrodes on top and bottom surfaces, which harvests mechanical energy in the longitudinal direction using the piezoelectric effect, as shown in Figure 2b. The piezoelectric effect is generated by the internal polarization induced by mechanical loads.[51] When stress, including normal stress (Figure 2b(i),(ii)) and shear stress (Figure 2b(iii)), is applied to the piezoelectric ceramic, the separation of the positive and negative gravity centers within the molecular structure results in dipoles that polarize the ceramic.[52] To neutralize the polarization effect, equal amounts of bound charges are generated on opposite surfaces, leading to the generation of current during the charge transfer. On the other hand, the tribo-module consists of Si and GaN, with indium (In) coated on the backside of Si and the surface of GaN as electrodes. It utilizes the tribovoltaic effect to collect mechanical energy in the transverse direction, as displayed in Figure 2c. The tribovoltaic effect generates a current contributed by the induced non-equilibrium electric field during the sliding.[53] The two semiconductors have different Fermi levels and surface states before contacting, and carriers in the n-region (GaN) are mainly electronic, while in the p-region (Si) they are primarily holes (Figure 2c(i)). Upon contact, carrier transfer occurs near the interface, leaving only the dopant ions to form a space charge region near the interface and create a built-in electric field E_{in} (Figure 2c(ii)). As the Si slides on the GaN, the asymmetrical space charge region leads to a non-equilibrium electric field ($E_{in} < E_1 + E_2$), allowing electrons and holes to flow along the external circuit and eventually reach a new electrical balance (Figure 2c(iii)). In this process, current can be generated in the external circuit to produce energy. By integrating the outputs from the piezo-module and the tribo-module through a switchable management circuit shown in Figure S4 (Supporting Information), the combined electrical output can be obtained, and separated outputs from two effects can also be distinguished (see the related movie in SV1, Supporting Information).

The energy generation capability of the combined P-TVNG system has been systematically studied, with a detailed analysis of the contributions as well as key factors influencing the performance of both the piezo-module and tribo-module. To fully demonstrate the function of the piezo-module, two operating modes, namely the single-piece mode (SP mode) and the multi-pieces mode (MP mode), are designed. The schematic and circuit diagram of these modes are shown in **Figure 3a(i)** (SP mode) and Figure 3a(ii) (MP mode), respectively. In the SP mode (Figure 3b), a PZT ceramic is attached to the back of the Si (or GaN), and two modules are connected in parallel to a single ammeter. Longitudinal force and transverse motion are applied by two-axis stepping motors. The SP mode offers the advantages of low cost, simple fabrication, and easy integration with the tribo-module, while the performance improvement of the SP mode is insufficient. Hence, based on the SP mode, the MP mode (Figure 3c) is

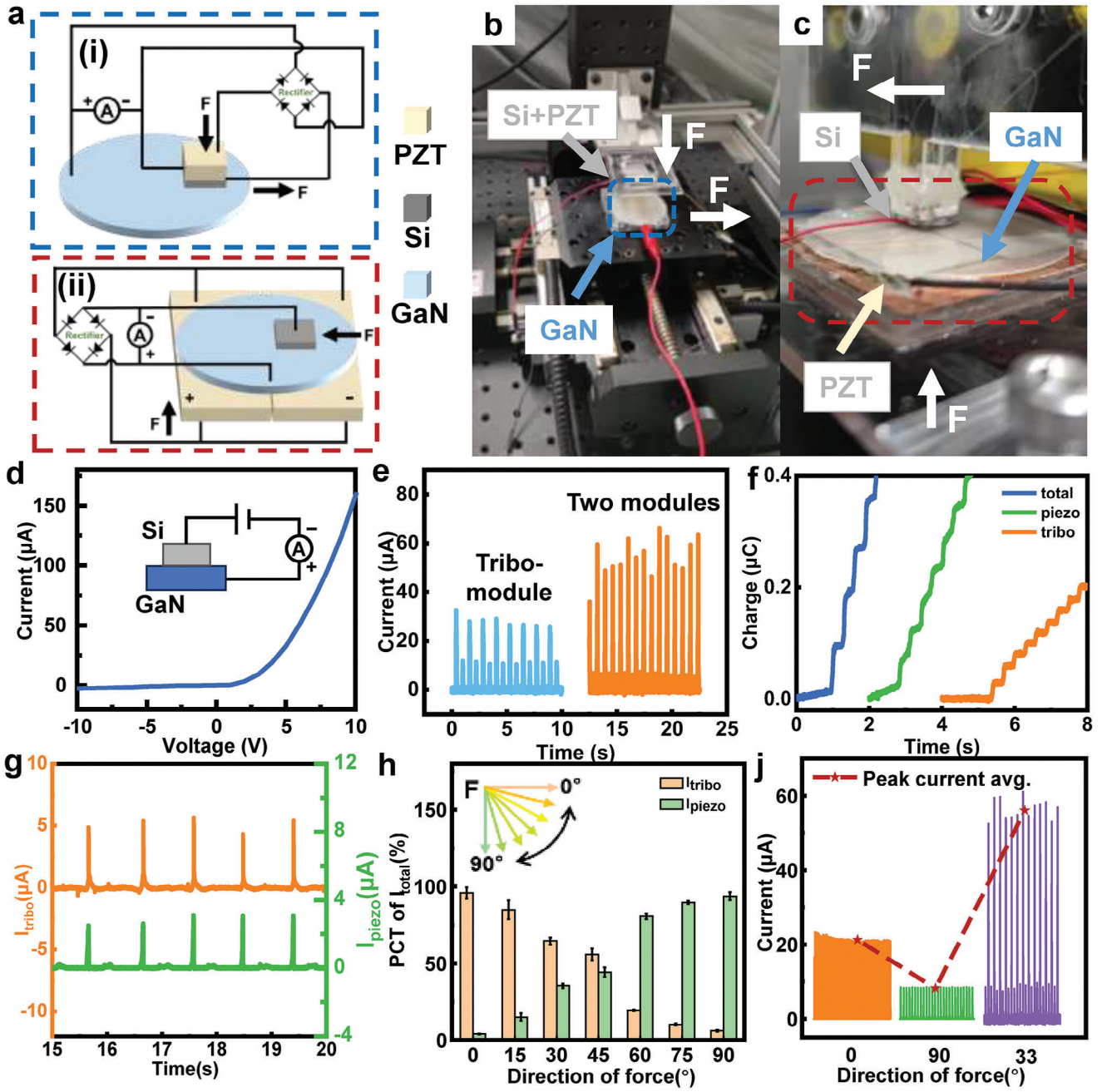

Figure 3. The working modes and the output of the P-TVNG system. a) The structure diagram of the SP mode (i) and the MP mode (ii). b and c) The detailed photographs of the SP mode (b) and the MP mode (c). d) I-V characteristic of the Si and GaN heterojunction. e) The comparison of the tribo-current and piezo/tribo-current. f) The transfer charge of the piezo-module, tribo-module and combined piezo/tribo-module for each cycle. g) The comparison for current curve of each module. h) The contribution to current of each module. j) The piezo/tribo-current at the 0°, 90°, and 33° direction of force.

developed to address the uneven distribution of the stress. The MP mode involves the use of multiple PZT ceramics attached to the back of the GaN (or Si), in accordance with the variation of applied stress in the vertical direction. Lateral motion is provided by a linear motor, and the longitudinal pressure is controlled by adjusting the height of a small lifting platform. Despite the design complexity, the MP mode offers the capability to fully harvest mechanical energy from complex working conditions, further improving the energy harvesting efficiency of the P-TVNG system.

Based on the above design, a comprehensive performance evaluation of the P-TVNG system is conducted. The I-V characteristic of the Si and GaN heterojunction (Figure 3d) demonstrates that when a forward bias is applied to Si, the output current exhibits exponential growth with voltage, indicating a favorable heterogeneous contact at the interface. A brief comparison

of the output current before and after the integration of the piezo-module in the MP mode is illustrated in Figure 3e, while a more detailed comparison of the piezo-module, tribo-module and the combined piezo/tribo-module is presented in Figure S5 (Supporting Information). At a vertical force of approximately 9 N and a maximum speed of 1 $m^{-1}s$, the combined piezo/tribo-current reaches approximately 60 μA, whereas the tribo-current alone is only 30 μA when the piezo-module is disconnected. Notably, the peak output current of the combined piezo/tribo-module exceeds the highest record for Si/GaN-type TVNGs that has ever been reported before. We have also measured the tribo-current and piezo-current as functions of normal pressure at a fixed sliding speed, where both outputs increase linearly before the Si film is crushed by the pressure. The comparison of the output voltage is also shown in Figure S6 (Supporting Information). It is noteworthy that although the total voltage actually decreases when the two modules work together, the power density of the combined piezo/tribo-module remains higher than that of either module working alone. Figure 3f presents the charge transfer curves for sliding in the forward and backward direction at a contact area of 1 cm^2, and it can be observed that the charge curves exhibit a stepped shape. The amount of charge transfer for three cases (piezo-module, tribo-module, and piezo/tribo-module together) is measured to be 0.04, 0.002, and 0.08 μC, respectively in a single cycle, indicating a significant enhancement in the charge transfer of the system. Figure 3g describes the output current of the two modules measured separately by two ammeters, and the simultaneous occurrence of peaks indicates that the combination of the two modules has a synergistic effect on the current. Both results are obtained under non-optimal operating conditions, demonstrating that the superposition of signals still exists in general and that the synergy of the two effects is naturally achievable.

Then, the output current of each module is evaluated in the SP mode, represented as a percentage contribution to the total current, under the application of resultant forces ranging from horizontal (0°) to vertical (90°), as depicted in Figure 3h. As the vector angle of the applied force transitions from 0° to 90°, the contribution of the tribo-module diminishes while the contribution of the piezo-module increases. With an increase in the applied vertical pressure, the contribution of the piezo-module experiences a corresponding increase. Simultaneously, the frictional resistance between Si and GaN also intensifies, but the horizontal component force decreases, thereby reducing the propensity of sliding between the two materials. Therefore, the amount of carriers' migration reduces during the process of rebuilding a new electric balance, and the contribution of the tribo-module decreases. Beyond the applied force direction angle of 45°, sliding becomes increasingly difficult, resulting in a rapid decline in the contribution of the tribo-module. Moreover, it is worth noting that at 0° and 90°, the contribution value of the piezo-module and the tribo-module are not completely zero. The reason is that at 0°, the tangential force brought by the lateral movement also induces deformation in the piezoelectric ceramics. Meanwhile, the vertical squeezing at 90° causes strain in Si and GaN, and the potential barrier between the two decreases in the strained state, resulting in the directional movement of carriers and the current output (see details in Figure S7, Supporting Information).[54] In the comparison of the current measured in the MP mode at the vector angle of applied force of 0°, 90°, and 30° (see Figure 3j), the combined output current generated from mixed motion is significantly higher than that generated from single motion, indicating that at the optimal angle of 30° for the experiment, the P-TVNG system exhibits excellent performance in collecting energy in complex pressure and motion conditions.

To further elaborate on the improvement of the output performance of the P-TVNG, the impedance-matching curve and output power are measured in the MP mode, as shown in **Figure 4a**, with the test circuit shown in the inset. With the increasing of resistance, the current of P-TVNG gradually decreases, while the power density initially increases and then decreases. At 1 MΩ, the power density reaches a maximum value of 3.61 W m^{-2}, which is 64.09 % higher than that of the tribo-module (Figure S8, Supporting Information), and 28.93 % higher than the highest record of 2.8 W m^{-2} of Si/GaN-TVNG.[16] The comparison indicates that the P-TVNG device exhibits higher output power and lower impedance. In order to verify the charging performance of the P-TVNG, the device is directly connected with a capacitor in series. As revealed in Figure 4b, the voltage can reach 6 V for 3.68 s of charging 0.33 μF capacitor, which is ≈2 s faster than when the tribo-module works alone (the related movie can be seen in SV1, Supporting Information). Figure 4c presents the output power density of the representative TVNG devices reported in recent years, and this P-TVNG (Si/GaN based TVNG combined with PZT ceramic) updates the highest power. To further improve the output current of the P-TVNG, a stack PZT ceramic fabricated by tape-casting process is used as the piezo-module, and the detailed fabrication process is described in the Experimental Section (see Figure S9, Supporting Information). The stack PZT ceramic consists of 10 layers of PZT ceramic bonded together with silver electrode layers between each layer, as the detailed photograph and structure shown in Figure 4d and Figure S10a (Supporting Information). From the SEM image presented in Figure S10b (Supporting Information), the stack PZT ceramic has a uniform grain distribution and is tightly bonded. The material parameters of the d_{33}-PZT ceramic, d_{15}-PZT ceramic and the stack PZT ceramic are listed in Table S1 (Supporting Information). Then, measured in the SP mode, the current of the P-TVNG has been significantly boosted while the voltage has dropped to a very low value because of the the parallel connection of multiple PZT ceramics in the stack, as shown in Figure 4e,f. The impedance-matching curve and output power are also measured, as shown in Figure S11 (Supporting Information), and the power density reduces by two orders of magnitude compared to the device utilizing d_{33}-PZT ceramic. Herein, the stack PZT ceramic is only suitable for applications requiring high current output.

Differing from the normal motor or actuator that requires the smooth surfaces for frictional motion, the tribovoltaic effect requires interfaces to be in close contact or even extruded against each other to induce an internal electric field. In this case, resolving the complex stress variation at the interface can guide the design of tribovoltaic devices, and the piezo-module of the P-TVNG system can be very suitable for this purpose. Stresses at the interface can be conducted through the tribovoltaic material and sensed by the piezo-module settled on the backside of the tribovoltaic materials.

By switching the management circuit, the P-TVNG system can transition from an energy harvesting function to sensing function. In the SP mode, the energy generation process of the TVNG

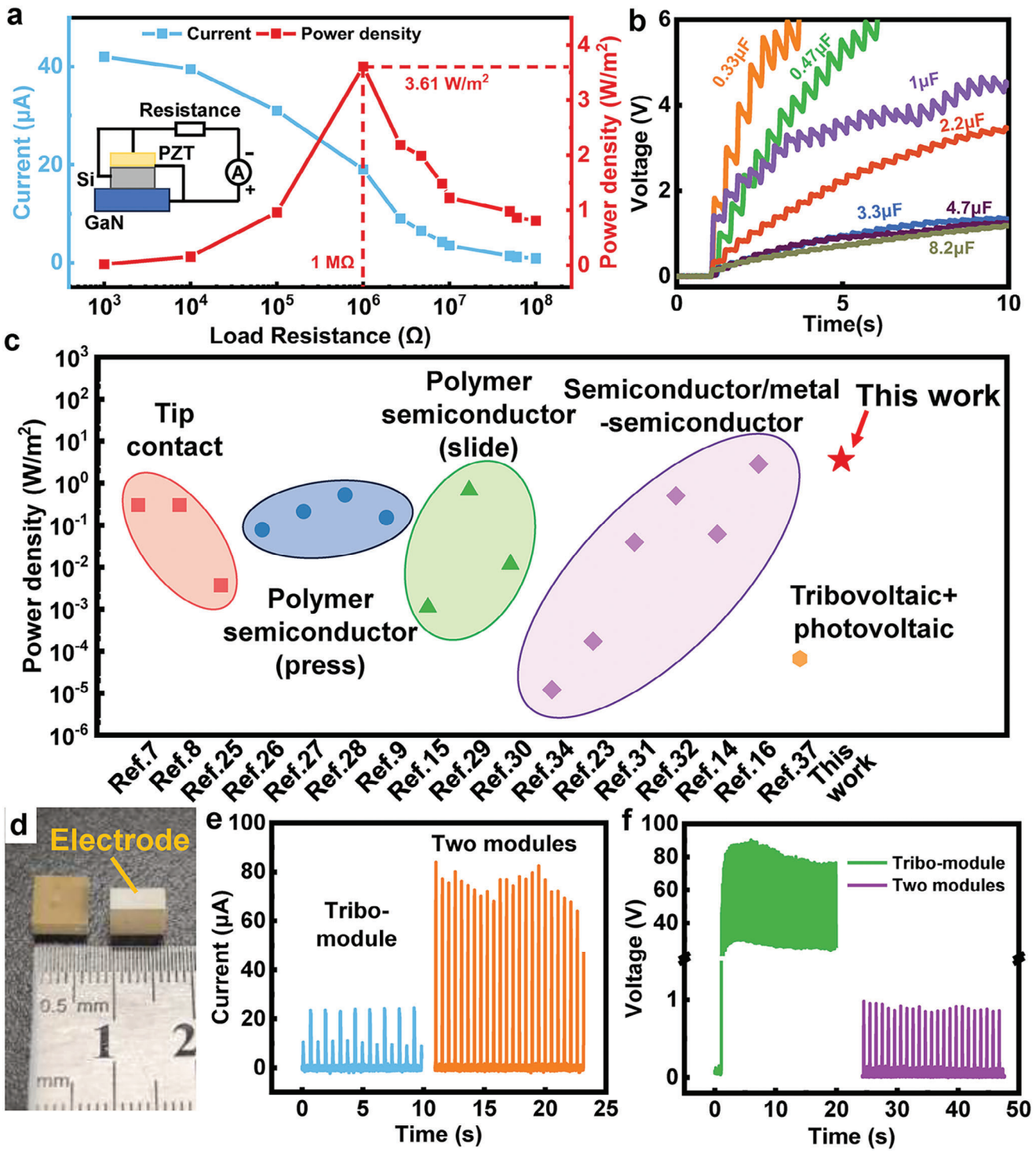

Figure 4. The output performance of the P-TVNG system. a) The output current and power density of the P-TVNG with various loads. b) Charging characteristics of the P-TVNG with different capacitors. c) Comparison of the power density with different type of TVNGs. d) The detailed photograph of the stack PZT ceramic. e) The comparison of the tribo-current and piezo/tribo-current with the stack PZT ceramic as piezo-module. f) The comparison of the tribo-voltage and piezo/tribo-voltage with the stack PZT ceramic as piezo-module.

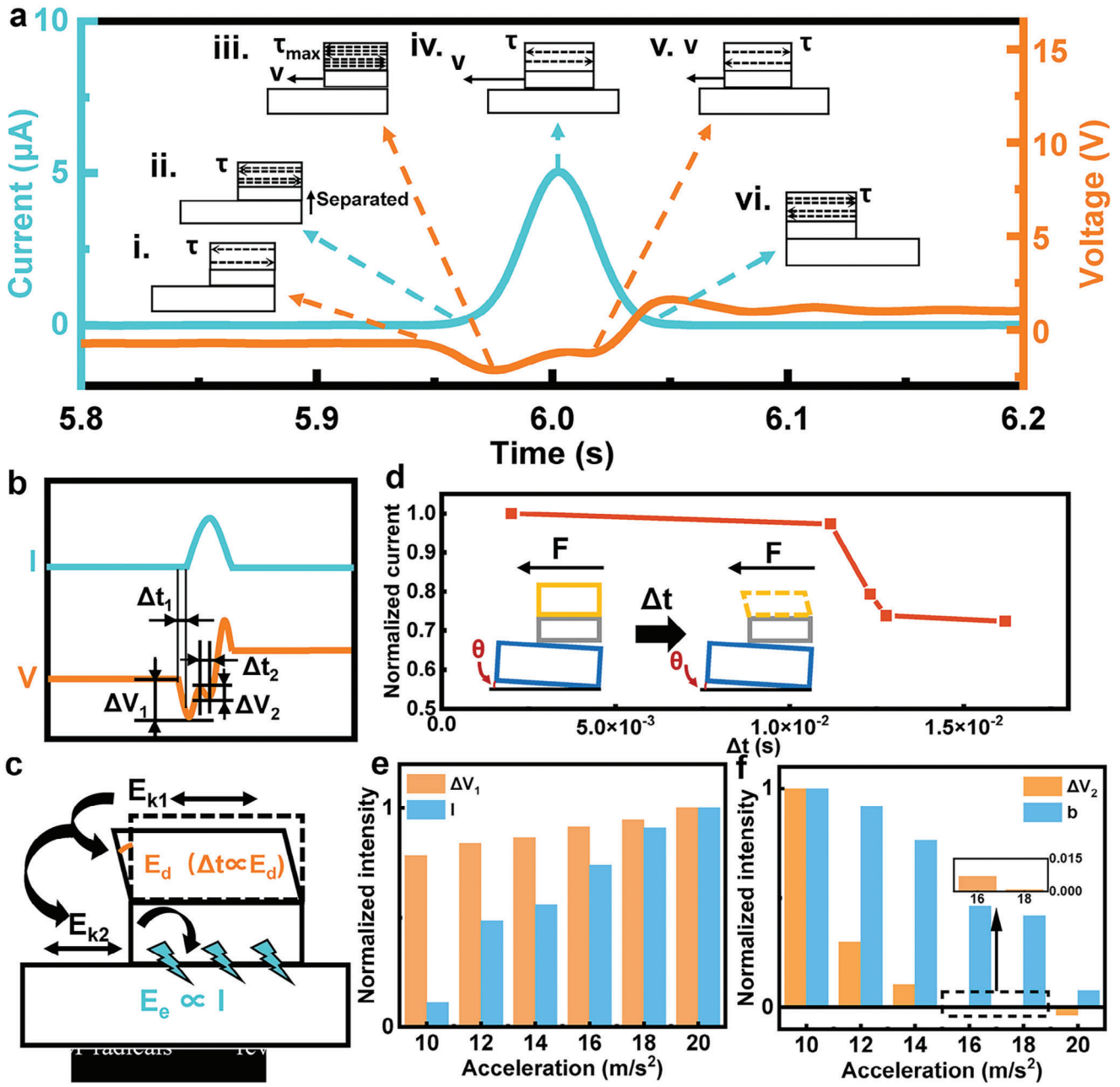

Figure 5. Sensory signal of the P-TVNG system. a) The waveform of the piezo-voltage and tribo-current and schematic diagram of the state of motion in a sliding cycle. b) Eigenvalues for resolving sensed signals. c) The energy conversion process of the P-TVNG. d) The normalized I–Δt_1 curve with different θ. e) The normalized ΔV_1 and I with different accelerations of motor. f) The normalized ΔV_2 and b in the decelerate process under different accelerations.

can be divided into six stages based on the vibration of tribo-current and piezo-voltage signals in one cycle of sliding, as depicted in **Figure** 5a. First, at stage i), the tribo-current remains zero and the piezo-voltage starts to show up. When the linear motor is initially active, the Si and GaN interface is subjected to the static friction, resulting in the shear force applied to the PZT ceramic and the generation of piezo-voltage. Next, at stage ii), the tribo-current starts to show up and the piezo-voltage keeps increasing. The applied force continues to increase and the PZT ceramic is subjected to a greater shear force, leading to a larger piezo-voltage. At Poisson's ratios of the PZT ceramic $\nu > 0$, the increase in the deformation of the ceramic leads to a decrease in thickness, driving the separation of Si from GaN, resulting in a decrease in E_{in} and the generation of tribo-current. At stage iii), the tribo-current increases and the piezo-voltage reaches the peak value. The applied force gradually increases to the maximum static friction, at which point the ceramic reaches its maximum deformation. Subsequently, at stage iv), the tribo-current reaches

the peak value and the piezo-voltage decreases to a plateau. At this stage, the sliding speed increases to the maximum, leading to the largest tribo-current. Meanwhile, the sliding friction at the interface is smaller than the maximum static friction, resulting in a decrease in piezo-voltage. Moving on to stage v), the tribo-current decreases and the piezo-voltage increases in reverse. As the deceleration stage begins, the decrease in sliding speed causes the decrease of tribo-current. Meanwhile, the top of the PZT ceramic is subjected to a braking force leading to the reverse shear and an increase in piezo-voltage. Finally, at stage vi), the tribo-current drops to zero and the piezo-voltage reaches the peak value in reverse. With the sliding stopped, the tribo-current generation returns to zero, while the shear of the ceramic reaches its maximum value, resulting in the peak piezo-voltage. It has been found that the change in tribo-current lags behind the increase in piezo-voltage, since the applied pressure always changes before displacement can occur, further confirming the necessity of integrating pressure energy collection. Then, there are different stress states in different positions on the GaN subtract, and thus, the baseline of piezo-voltage changes. The curve of the piezo-voltage in sliding backward mirrors the stages i–vi, as shown in Figure S12 (Supporting Information).

Figure 5b illustrates a simplified schematic of the waveform, with arrows labeling the characteristic values that can be used to characterize the working condition of the system. In this schematic, Δt_1 represents the time difference between the start of the voltage and the start of the current. ΔV_1 indicates the difference between the peak piezo-voltage and the baseline before the sliding. ΔV_2 represents the difference between the lowest value of piezo-voltage drops and the peak of piezo-voltage mutation before deceleration. Finally, Δt_2 signifies the time of the piezo-voltage mutation.

During the P-TVNG working, an energy conversion process happens as follow:

$$E_{k1} = E_d + E_{k2} \tag{1}$$

where E_{k1} is the input kinetic provide by the linear motor, E_d is the deformation potential of PZT ceramic, and E_{k2} is kinetic of Si sliding on GaN. During the time of Δt_1, the deformation (D) of the PZT ceramic can be calculated as:

$$D = \int_0^{\Delta t_1} dt \int \frac{F(t)}{m} dt \tag{2}$$

where $F(t)$ is the function of the force, which is set in the experiment as $F(t) = 5000t$, m is the mass of the moving block of the motor. For E_d, there is:

$$E_d = \frac{1}{2} k\gamma^2 \tag{3}$$

where $k = E(1+\nu)/2$ is deformation potential constant, ν is the Poisson's ratio of PZT ceramic, and $\gamma = \frac{D}{t}$ is shear strain (t: thickness of PZT ceramic). Because of the tribovoltaic effect, E_{k2} is transformed into the output electrical energy E_e, and for E_e, there is:

$$E_e = \int I^2(t) R dt \tag{4}$$

where R is the resistance. Therefore, by associating the above equations, the final Δt_1 is negatively correlated with the peak current I:

$$I \propto \frac{1}{\Delta t_1} \tag{5}$$

The whole energy conversion process is shown in Figure 5c. Figure 5d describes the normalized I–Δt_1 curve and the I decreases with an increase in Δt_1, where Δt_1 is varied by changing the angle θ between the substrate and the horizontal plane in the initial state under the same force, as depicted in the inset. As θ increases to the point where Si breaks up in sliding due to the excessive stress, the I at max θ drops to 70 % of that under ideal condition.

By adjusting the acceleration of the linear motor, the applied force on the system can be controlled, as depicted in Figure S13 (Supporting Information), which showcases the curves of the tribo-current and piezo-voltage at different accelerations. The characteristic parameters ΔV_1 and ΔV_2 are significantly different for different accelerations, indicating the influence of force variations on the operating state of the system. Figure 5e reveals the variations of ΔV_1 and peak tribo-current I under different accelerations, where ΔV_1 and I demonstrate synchronization and both increase with acceleration. ΔV_1 represents the maximum shear force applied to the P-TVNG system during the acceleration process, which is determined by the combination of the external force and the friction at the interface between Si and GaN. With higher acceleration, a greater speed is obtained, resulting in larger displacement variations per unit time, i.e., a larger I. The synchronization between the two parameters directly indicates that the external force, which enhances lateral motion, has a positive impact on the energy harvesting of the TVNG. Figure 5f demonstrates the variations of ΔV_2 and the absolute value of the slope (b) of the tribo-current during Δt_2 under different accelerations, where both ΔV_2 and b decrease as acceleration increases. When a high speed is set for the motor, a smaller acceleration can cause the system to directly enter the deceleration process before reaching a stage of uniform motion, resulting in a sudden change in force. This sudden change in force destabilizes the ceramic and Si to destabilize during sliding, reducing the contact area between Si and GaN, leading to a sharp decrease in tribo-current reflected by b and a sudden change in piezo-voltage reflected by ΔV_2. This result suggests that states with smoother force variations are more conducive to tribo-current output, whereas states with abrupt force changes lead to additional piezo-output. It further suggests that the boosts of output of the piezo-module and tribo-module are incompatible, but there is an optimized condition that allows the system to achieve the highest output performance.

In the subsequent sections, the potential applications of P-TVNG are demonstrated and envisioned. Among the various application scenarios, one notable use case involves the polishing process of GaN wafers. **Figure 6**a,b present the model and photograph used for simulation, respectively, illustrating the combination of Si, PZT ceramic, and the polishing head for contacting GaN during the polishing process. For the rotating P-TVNG, the smoothed piezo-voltage curves (Figure S14, Supporting Information) reveal that changes in stresses primarily occur during the starting and stopping processes, where larger rotational speeds

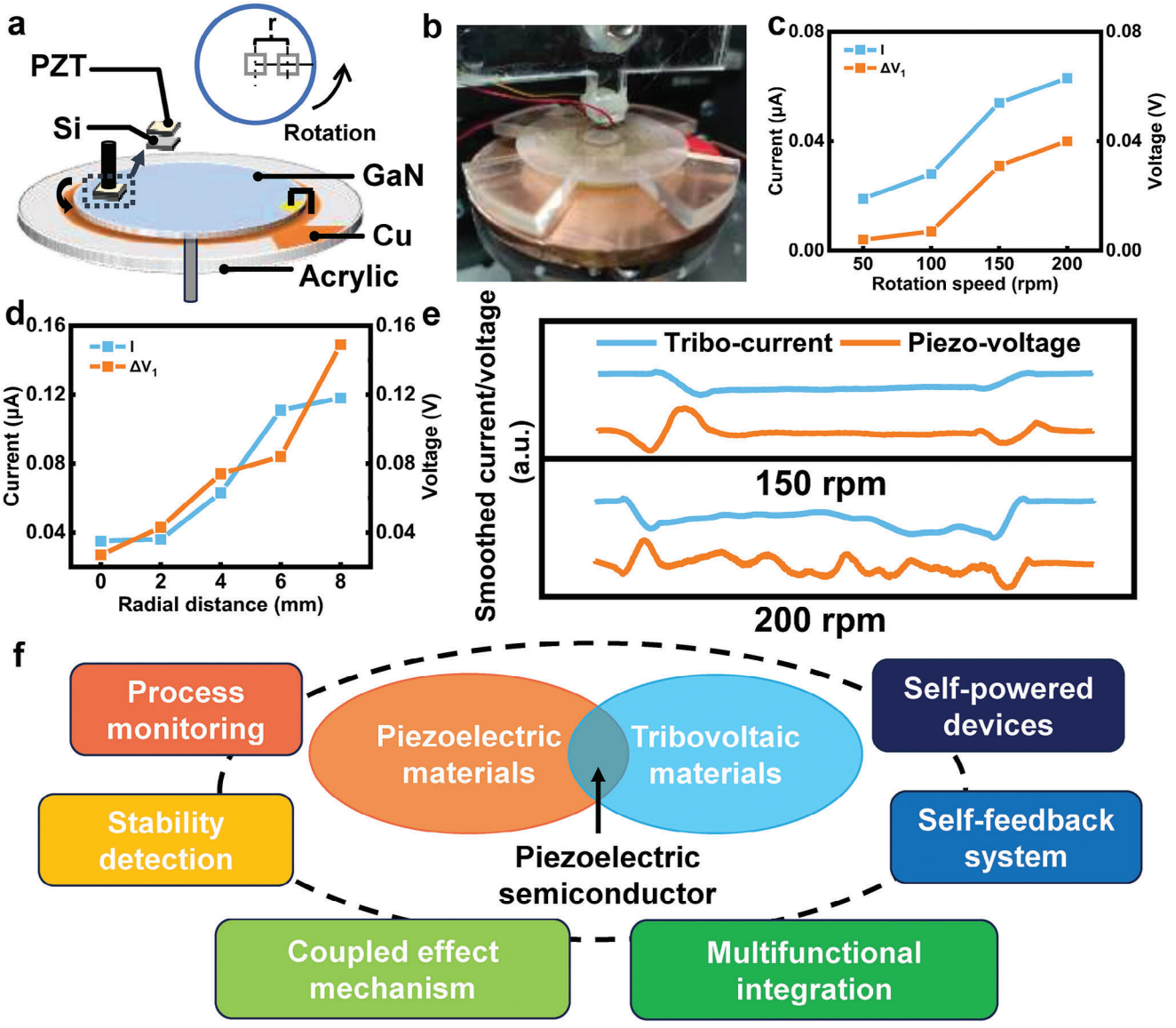

Figure 6. The application and prospects of the P-TVNG system. a,b) Simulation of P-TVNG in the polishing process. c) The ΔV_1 and I with different rotation speeds of motor. d) The ΔV_1 and *I* with different radial distance from the rotation center. e) The smoothed curves of tribo-current and piezo-voltage at the rotation speed of 150 rpm and 200 rpm. f) The prospect of P-TVNG system applying in sensory, self-power and multifunctional devices.

and radial distances correspond to greater accelerations, resulting in higher piezo-voltage and tribo-current (see Figure 6c,d, respectively). During smooth operation, a high and stable tribo-current can be obtained, whereas unsteady operation leads to a decrease in tribo-current (see Figure 6e). The utilization of tribo-current during the polishing process enables efficient energy recovery, while the use of the sensing function of the piezo-module also facilitates real-time monitoring of the polishing process. Furthermore, as illustrated in Figure 6f, the P-TVNG system holds immense potential for utilization in the field of recycling tiny energy and microdevices, owing to its high output performance, sensory function, and adaptability of the working mode. Moreover, as the demand for multifunctional devices continues to grow, the P-TVNG system presents a viable approach to integrate the piezoelectric effect and tribovoltaic effect into conventional semiconductor devices, leading the way for the development of new types of devices that encompass self-power, sensing, and self-regulation capabilities.

3. Conclusion

In summary, a P-TVNG system combining the piezoelectric effect and the tribovoltaic effect has been proposed, which integrates the function of high energy harvesting and dynamic pressure sensing. Two working modes of the piezo-module with single or multiple ceramic pieces are introduced to accommodate a wide range of conditions. Hence, this design concept allows the piezo-module to provide extra performance enhancement on the top of the original output limit of all kinds of TVNGs. The optimal working condition under the experimental system

is determined as a vertical force of 9 N, speed of 1 m^{-1} s, and combined force direction of ≈30° from the horizontal. The maximum output piezo/tribo-current of this P-TVNG system is up to 60 μA in the optimal condition, which is twice as much as that from the tribo-module only. The output power density is up to 3.61 W m−^{2}, which is 28.93 % higher than the highest record of the previous TVNG using the similar materials. Moreover, the piezo-module in this P-TVNG system can also work as a sensor device by switching the management circuit. Based on the piezo-voltage signals, the detailed operation characteristics of the TVNG can be analyzed. It has been found that the change in tribo-current lags behind the increased piezo-voltage and the different stress distribution at different stop positions can be revealed by the piezo-voltage signal. Moreover, the stable stress applied on top of device is conducive for TVNG to obtaining high tribo-current, while the variation of applied stress can cause significant output of piezo-module. Hence, the P-TVNG, as the integration of piezoelectric materials and semiconductors, can fully realize the multifunctionality of energy harvesting, sensing, and self-driving. This combined system can be applied for smart electromechanical systems and semiconductor manufacturing, where vertical contacts and sliding motions between different semiconductors are inevitable.

4. Experimental Section

Materials: The GaN wafers with the diameter of 2 inch were purchased from Shanghai GaNova Electronic Information Co., Ltd., China, and the layers from bottom to top were sapphire (430 μm), GaN buffer layer (50 nm) and ultralow-doped GaN (4.5 μm), as shown in Figure S1a (Supporting Information). The surface of the GaN was polished with a 6 μm diamond polishing paste and then cleaned with alcohol and deionized water. Pure metal indium covered the area of ≈1 cm^2 on the GaN surface as the electrode. The floating-zone silicon wafers were purchased from Kaihua Jingxin Electronic Co., Ltd., China, and were cut into several 10 × 10 mm pieces. The back of Si pieces was covered by indium as well. The PZT ceramics with silver electrode were purchased from Dongguan Jiaming Electronic Hardware Products Co., Ltd., China, and the sizes of the d_{33}-PZT was 10 × 10 × 2 mm and 40 × 40 × 1 mm while the size of the d_{15}-PZT is 8 × 8 × 0.5 mm.

Fabrication of Stack PZT Ceramic: The fabrication process of the stack PZT ceramic was illustrated in Figure S9 (Supporting Information). For the preparation of the PZT ceramic, PbO, $SrCO_3$, ZrO_2, TiO_2, $BaCO_3$, Nb_2O_3, SnO_2, and La_2O_3 were used, all of which were purchased from Sinopharm Chemical Reagent Co., Ltd. Initially, the powders were weighted according to the weight percentages shown in Table S2 (Supporting Information) and then ball milled with anhydrous ethanol at 360 rpm for 4 h. Subsequently, the mixture was dried at 60 °C for 8 h. The dried ceramic powder was then calcined after grinding. The temperature was maintained at 940 °C for 4 h and then lowered to 500 °C. The powder was further ball milled with PVB adhesive at 360 rpm for 6 h. After repeating the drying and grinding steps, the ceramic powder was obtained. Next, the ceramic powder, deionized water, and acrylic acid were roller milled at 300 rpm for 24 h. Then, a moistener (Surfynol SE-F) was added, and the mixture was roller milled at 300 rpm for 24 h. Polyvinyl alcohol and glycerine were subsequently added, and the mixture was roller milled together at 300 rpm for 24 h to fabricate the slurry. The slurry was then poured into the casting machine (LYJ-150) to cast wet belts of the PZT ceramic. After curing, the PZT ceramic blank film with a thickness of 0.3 mm was obtained through the following sintering processes: the temperature was raised from room temperature to 250 °C and held for 1 h; then raised to 600 °C and held for 2 h, next raised to 1200 °C and held for 2 h, and finally cooled down to 500 °C followed by free cooling. Subsequently, silver electrodes were imprinted onto the surface of the blank film through screen printing. The next step involves bonding the 10 layers of PZT ceramic film to create a stack PZT ceramic through pressing. The stack was then cut into blocks with the dimensions of 7 × 7 × 3 mm using a cutting machine (ACC-200A). Finally, the stack PZT ceramic was immersed in silicone oil at 120 °C and poled at 4 kV mm^{-1} for 15 min. The electric field was maintained until the ceramic cooled to 60 °C.

Experiment and Measurement: The frictional motion of Si was controlled by a linear motor, simultaneous application of normal stress and lateral motion by a two-axis motor, and the rotational motion of GaN was controlled by a step motor. Voltage and current were measured by a Keithley 6514. The force was tested by a force gauge (Handpi/HP-10). The photos of surface microstructure of GaN and Si were shot by scanning electron microscope (Hitachi SU8020). The surface morphologies of GaN and Si were scanned by atomic force microscopy (Asylum Research MFP-3D).

Supporting Information

Supporting Information is available from the Wiley Online Library or from the author.

Acknowledgements

This work was supported by the National Natural Science Fund of China for Excellent Young Scholar (52322313), National Key R&D Project from Minister of Science and Technology (2021YFA1201601), National Natural Science Fund of China (62174014), Beijing Nova program (Z201100006820063), Youth Innovation Promotion Association CAS (2021165), Innovation Project of Ocean Science and Technology (22-3-3-hygg-18-hy), State Key Laboratory of New Ceramic and Fine Processing Tsinghua University (KFZD202202), Fundamental Research Funds for the Central Universities (292022000337), Young Top-Notch Talents Program of Beijing Excellent Talents Funding (20170000021223ZK03).

Conflict of Interest

The authors declare no conflict of interest.

Data Availability Statement

The data that support the findings of this study are available from the corresponding author upon reasonable request.

Keywords

energy harvesting, integrated system, piezoelectric effect, sensor, tribovoltaic effect

Received: September 14, 2023
Revised: October 19, 2023
Published online: November 21, 2023

[1] F.-R. Fan, Z.-Q. Tian, Z. Lin Wang, *Nano Energy* **2012**, *1*, 328.
[2] Z. Liu, Y. Huang, Y. Shi, X. Tao, H. He, F. Chen, Z.-X. Huang, Z. L. Wang, X. Chen, J.-P. Qu, *Nat. Commun.* **2022**, *13*, 4083.
[3] P. Yang, Y. Shi, X. Tao, Z. Liu, X. Dong, Z. L. Wang, X. Chen, *Matter* **2023**, *6*, 1295.
[4] Z. Liu, Y.-Z. Huang, Y. Shi, X. Tao, P. Yang, X. Dong, J. Hu, Z.-X. Huang, X. Chen, J.-P. Qu, *Adv. Funct. Mater.* **2023**, *33*, 2302164.

[5] X. Tao, X. Chen, Z. L. Wang, *Energy Environ. Sci.* **2023**, *16*, 3654.
[6] P. Yang, Y. Shi, S. Li, X. Tao, Z. Liu, X. Wang, Z. L. Wang, X. Chen, *ACS Nano* **2022**, *16*, 4654.
[7] J. Liu, A. Goswami, K. Jiang, F. Khan, S. Kim, R. Mcgee, Z. Li, Z. Hu, J. Lee, T. Thundat, *Nat. Nanotechnol.* **2018**, *13*, 112.
[8] J. Liu, M. Miao, K. Jiang, F. Khan, A. Goswami, R. Mcgee, Z. Li, L. Nguyen, Z. Hu, J. Lee, K. Cadien, T. Thundat, *Nano Energy* **2018**, *48*, 320.
[9] H. Shao, J. Fang, H. Wang, L. Dai, T. Lin, *Adv. Mater.* **2016**, *28*, 1461.
[10] J. Liu, K. Jiang, L. Nguyen, Z. Li, T. Thundat, *Mater. Horiz.* **2019**, *6*, 1020.
[11] Y. Lu, S. Feng, R. Shen, Y. Xu, Z. Hao, Y. Yan, H. Zheng, X. Yu, Q. Gao, P. Zhang, S. Lin, *Research* **2019**, *2019*, 5832382.
[12] S. Lin, Y. Lu, S. Feng, Z. Hao, Y. Yan, *Adv. Mater.* **2019**, *31*, 1804398.
[13] Y. Lu, Z. Hao, S. Feng, R. Shen, Y. Yan, S. Lin, *iScience* **2019**, *22*, 58.
[14] J. Liu, M. I. Cheikh, R. Bao, H. Peng, F. Liu, Z. Li, K. Jiang, J. Chen, T. Thundat, *Adv. Electron. Mater.* **2019**, *5*, 1900464.
[15] J. Meng, Z. H. Guo, C. Pan, L. Wang, C. Chang, L. Li, X. Pu, Z. L. Wang, *ACS Energy Lett.* **2021**, *6*, 2442.
[16] Z. Wang, Z. Zhang, Y. Chen, L. Gong, S. Dong, H. Zhou, Y. Lin, Y. Lv, G. Liu, C. Zhang, *Energy Environ. Sci.* **2022**, *15*, 2366.
[17] A. Sutka, M. Zubkins, A. Linarts, L. Lapcinskis, K. Ma?Lnieks, O. Verners, A. Sarakovskis, R. Grzibovskis, J. Gabrusenoks, E. Strods, K. Smits, V. Vibornijs, L. Bikse, J. Purans, *J. Phys. Chem. C* **2021**, *125*, 14212.
[18] Z. Zhang, T. He, J. Zhao, G. Liu, Z. L. Wang, C. Zhang, *Mater. Today Phys.* **2021**, *16*, 100295.
[19] J. Liu, F. Liu, R. Bao, K. Jiang, F. Khan, Z. Li, H. Peng, J. Chen, A. Alodhayb, T. Thundat, *ACS Appl. Mater. Interfaces* **2019**, *11*, 35404.
[20] X. Yu, H. Zheng, Y. Lu, R. Shen, Y. Yan, Z. Hao, Y. Yang, S. Lin, *RSC Adv.* **2021**, *11*, 19106.
[21] S. Lin, R. Shen, T. Yao, Y. Lu, S. Feng, Z. Hao, H. Zheng, Y. Yan, E. Li, *Adv. Sci.* **2019**, *6*, 1901925.
[22] Z. L. Wang, A. C. Wang, *Mater. Today* **2019**, *30*, 34.
[23] M. Benner, R. Yang, L. Lin, M. Liu, H. Li, J. Liu, *ACS Appl. Mater. Interfaces* **2022**, *14*, 2968.
[24] R. Xu, Q. Zhang, J. Y. Wang, D. Liu, J. Wang, Z. L. Wang, *Nano Energy* **2019**, *66*, 104185.
[25] S. Deng, R. Xu, W. Seh, J. Sun, W. Cai, J. Zou, Q. Zhang, *Nano Energy* **2022**, *94*, 106888.
[26] H. Shao, J. Fang, H. Wang, H. Zhou, H. Niu, F. Chen, G. Yan, S. Fu, Y. Cao, T. Lin, *Adv. Electron. Mater.* **2019**, *5*, 1800675.
[27] H. Shao, J. Fang, H. Wang, H. Niu, H. Zhou, Y. Cao, F. Chen, S. Fu, T. Lin, *Nano Energy* **2019**, *62*, 171.
[28] W. Wang, X. Han, J. Niu, X. Jin, H. Wang, H. Shao, T. Lin, *J. Mater. Chem. A* **2020**, *8*, 24166.
[29] R. Yang, M. Benner, Z. Guo, C. Zhou, J. Liu, *Adv. Funct. Mater.* **2021**, *31*, 2103132.
[30] Z. You, S. Wang, Z. Li, Y. Zou, T. Lu, F. Wang, B. Hu, X. Wang, L. Li, W. Fang, Y. Liu, *Nano Energy* **2022**, *91*, 106667.
[31] B. Fan, Z. Wang, G. Liu, Z. Wang, X. Fu, L. Gong, C. Zhang, *Adv. Funct. Mater.* **2023**, *33*, 2301821.
[32] Y. Chen, Z. Zhang, Z. Wang, T. Bu, S. Dong, W. Wei, Z. Chen, Y. Lin, Y. Lv, H. Zhou, W. Sun, C. Zhang, *ACS Appl. Mater. Interfaces* **2022**, *14*, 24020.
[33] X. Xu, J. Li, X. Tao, Q. Yan, H. Wu, Z. Guan, L. Liu, X. Chen, W. Ou-Yang, *Nano Energy* **2022**, *94*, 106957.
[34] Z. Zhang, Z. Wang, Y. Chen, Y. Feng, S. Dong, H. Zhou, Z. L. Wang, C. Zhang, *Adv. Mater.* **2022**, *34*, 2200146.
[35] Y. Wang, G. Zhang, H. Wu, B. Sun, *Adv. Energy Mater.* **2021**, *11*, 2100578.
[36] H. Yuan, Z. Xiao, J. Wan, Y. Xiang, G. Dai, H. Li, J. Yang, *Adv. Energy Mater.* **2022**, *12*, 2200550.
[37] Z. Hao, T. Jiang, Y. Lu, S. Feng, R. Shen, T. Yao, Y. Yan, Y. (.M.). Yang, Y. Lu, S. Lin, Y. (Michael) Yang, Y. Lu, S. Lin, *Matter* **2019**, *1*, 639.
[38] L. Ren, A. Yu, W. Wang, D. Guo, M. Jia, P. Guo, Y. Zhang, Z. L. Wang, J. Zhai, *Nano Lett.* **2021**, *21*, 10099.
[39] V. A. Sharov, P. A. Alekseev, B. R. Borodin, M. S. Dunaevskiy, R. R. Reznik, G. E. Cirlin, *ACS Appl. Energy Mater.* **2019**, *2*, 4395.
[40] C. Ma, B. Kim, S.-W. Kim, N.-G. Park, *Energy Environ. Sci.* **2021**, *14*, 374.
[41] S. Saadon, O. Sidek, *Energy Convers. Manag.* **2011**, *52*, 500.
[42] X. Gao, J. Wu, Y. Yu, Z. Chu, H. Shi, S. Dong, *Adv. Funct. Mater.* **2018**, *28*, 1706895.
[43] X. Gao, J. Wu, Y. Yu, S. Dong, *Appl. Phys. Lett.* **2017**, *111*, 212904.
[44] J. Wu, X. Chen, Z. Chu, W. Shi, Y. Yu, S. Dong, *Appl. Phys. Lett.* **2016**, *109*, 173901.
[45] L. Yang, X. Kong, F. Li, H. Hao, Z. Cheng, H. Liu, J.-F. Li, S. Zhang, *Prog. Mater. Sci.* **2019**, *102*, 72.
[46] Y. Liao, H. Yang, Q. Liao, W. Si, Y. Chu, X. Chu, L. Qin, *Coatings* **2023**, *13*, 1252.
[47] T. Sharma, S.-S. Je, B. Gill, J. X. J. Zhang, *Sens. Actuators Phys.* **2012**, *177*, 87.
[48] X. Chen, Q. Zeng, J. Shao, S. Li, X. Li, H. Tian, G. Liu, B. Nie, Y. Luo, *ACS Appl. Mater. Interfaces* **2021**, *13*, 34637.
[49] H. Cui, R. Hensleigh, D. Yao, D. Maurya, P. Kumar, M. G. Kang, S. Priya, X. Zheng, *Nat. Mater.* **2019**, *18*, 234.
[50] K. Okazaki, K. Nagata, *J. Am. Ceram. Soc.* **1973**, *56*, 82.
[51] D. Y. Gao, R. W. Ogden, *An Introduction to the Theory of Piezoelectricity*, Kluwer Academic Publishers, Boston **2005**.
[52] K. A. Cook-Chennault, N. Thambi, M. A. Bitetto, E. B. Hameyie, *Bull. Sci. Technol. Soc.* **2008**, *28*, 496.
[53] X. Huang, X. Xiang, J. Nie, D. Peng, F. Yang, Z. Wu, H. Jiang, Z. Xu, Q. Zheng, *Nat. Commun.* **2021**, *12*, 2268.
[54] B. Gil, P. Lefebvre, H. Morkoç, *Comptes Rendus Académie Sci. – Ser. IV – Phys.* **2000**, *1*, 51.

